




Kinetic analysis of the formation of high-temperature phases in an illite-based ceramic body using thermodilatometry

Tomáš Ondro¹ · Tomáš Húlan¹ · Omar Al-Shantir¹ · Štefan Csáki^{2,3} · Tereza Václavů⁴ · Anton Trník^{1,5} 

Received: 29 October 2018 / Accepted: 1 September 2019 / Published online: 12 September 2019
© Akadémiai Kiadó, Budapest, Hungary 2019

Abstract

A non-isothermal kinetic analysis of the sintering process of an illitic clay is studied by thermodilatometry. For this study, illitic clay with over 80 mass% of illite content, originated in the Füzérradvány location in northeastern Hungary, is used as basic material. The measurements are performed using a push-rod dilatometer on compact samples with heating rates from 1 to 10 °C min⁻¹ in dynamic N₂ atmosphere. The Kissinger method is used for the parameterization of the process. The results show that the reaction sintering runs in several overlapping steps. The determined values of the apparent activation energy of the first step and second step are $E_A = (625 \pm 18)$ kJ mol⁻¹ and $E_A = (575 \pm 14)$ kJ mol⁻¹, respectively. The results also show that both reactions could be characterized by the thickening of long cylinders (needles) or growth of needles and plates of finite long dimensions.

Keywords Kinetics · Illite · Sintering · Apparent activation energy

Introduction

A group of ceramic materials that are sometimes called “traditional ceramics” is based on the utilization of naturally occurring clay minerals. Products belonging to the group of traditional ceramics include porcelain, bricks, floor and roof tiles, sewer pipes, etc. Among many kinds of clay minerals, kaolinite and illite are most frequently found in raw clays and usually they also are a major part of those clays. Kaolinitic clays are essential for porcelain

production, while illitic clays are more often used as a basic material for products of building ceramics.

The technological process of traditional ceramics production consists of clay mining, its purification, mixing with other additives, shaping of product, drying, firing and, sometimes, glazing and grinding [1]. Among these processes, the firing is the most important step. It is a sequence of heating to a required temperature with a specific heating rate, isothermal regime at a higher temperature and cooling down to room temperature with a specific cooling rate. During firing, the final properties of the ceramic product are obtained, such as mechanical strength, hardness, chemical and microstructural durability, refractoriness or color. The most significant changes in clay minerals occur, when they are thermally treated and include drying, dehydroxylation, structural collapse and formation of new minerals either directly from the collapsed structure (i.e., spinel formation from metakaolinite) or from the melt. From the perspective of ceramics production, the most significant stage of firing is sintering, which occurs at the highest applied temperature. In this stage, powder particles, which form the green body, are interconnected either by the action of melted phase or sintering in solid state or by reaction sintering accompanied by the formation of new mineralogical phases [2].

✉ Anton Trník
atrnik@ukf.sk

¹ Department of Physics, Constantine the Philosopher University in Nitra, Tr. A. Hlinku 1, 949 74 Nitra, Slovakia

² Department of Physics of Materials, Charles University, Ke Karlovu 5, 121 16 Prague, Czech Republic

³ Institute of Plasma Physics, Czech Academy of Sciences, Za Slovankou 3, 182 00 Prague, Czech Republic

⁴ Department of Condensed Matter Physics, Charles University, Ke Karlovu 5, 121 16 Prague, Czech Republic

⁵ Department of Materials Engineering and Chemistry, Czech Technical University in Prague, Thákurova 7, 166 29 Prague, Czech Republic

Illite loses its structural water between 450 and 780 °C during the process known as *dehydroxylation* [3]. Its crystal structure after dehydroxylation, however, remains almost unchanged up to 850–950 °C [4–6]. Despite this, the first spots of liquid were observed already at the temperature of ~ 700 °C [7]. Because of the relatively high potassium content in illite (~ 7 mass%), it tends to form a high amount of melted phase [5, 6, 8]. In addition, after firing between 900 and 1000 °C, it creates potassium aluminosilicate glass [9]. Potassium cation significantly inhibits the formation of new minerals [4, 5]. The most often observed mineral phase developed from illite is mullite [4, 7–9] which begins to form in the temperature range from 1050 to 1150 °C. In [5], the formation of mullite was reported even at temperatures lower than 1000 °C. On the other hand, mullite was not observed in clay containing 40 mass% of illite and 15 mass% of chlorite fired at 1075 °C [6]. This was attributed to the high magnesium content. Another phase that is often observed after firing in the illitic clays is spinel. The temperatures at which spinel begins to form are between 1000 and 1100 °C [4, 7, 9]. Besides mullite and spinel, the formation of β -quartz in the temperature interval from 1000 to 1300 °C was observed in [4]. It was reported in [7] that high-temperature phases had preferential orientation depending on the orientation of the original clay particles. The results of various studies [5, 8, 10] indicated that the formation of high-temperature mineralogical phases in illitic clays is rather strongly dependent on the composition of original material. For example, illite acts as a precursor of cordierite crystallization if magnesium was present in the material [8].

The evolution of microstructure during the sintering is not given only by the inherent properties of the used materials, but in large extent also by the consolidation of particles during the shaping and drying process. Some studies [4, 5, 7, 9, 11] were dedicated to investigating the phase evolution of clay minerals on powder samples. These studies can yield valuable information. However, when studying the sintering process, a compact sample must always be used. The most frequently used methods for in situ study of the sintering process are therm dilatometric analysis (TDA) and dynamical mechanical analysis (DMA) [12–15]. These analyses can be used to evaluate the kinetic parameters of the sintering process. The kinetic analysis provides information about the underlying mechanisms occurring during the sintering process; therefore, its results can be used to optimize the firing process. There are quite many studies [12, 16, 17] focusing on the sintering kinetics of kaolinite clay. On the other hand, according to the authors' best knowledge, only one study has reported information about the kinetics of illite sintering [6]. The mechanism of the illite sintering identified in [6] was

viscous flow sintering with an apparent activation energy of ~ 100 kJ mol⁻¹.

The aim of this study is to describe the sintering process of an illite-based ceramic body. The kinetic data are collected from therm dilatometric analysis during non-isothermal conditions in an inert dynamic atmosphere. Individual steps of reaction sintering are separated by a peak separation procedure. The Kissinger method is used to calculate the apparent activation energies of individual reaction sintering steps, and the Avrami peak factor is used to determine the mechanisms of those steps.

Materials and methods

The raw material with major content of illite was firstly crushed and then milled in a planetary ball mill Retsch PM100 to obtain a powder with a size of grains less than 100 μm . The as-prepared powder was mixed with distilled water to obtain a plastic mass from which the cylindrical samples were prepared by a laboratory extruder. The diameter of the samples after open-air drying was ~ 14 mm. To reduce the thermal gradients during heating, the diameter of the samples was reduced to ~ 7 mm [18].

Therm dilatometric analysis was performed on the horizontal push-rod dilatometer Netzsch DIL 402 C in dynamic N₂ atmosphere with the flow rate of 40 mL min⁻¹. The measurements were carried out in temperature interval from 40 °C to 1300 °C with heating rates of 1, 3, 5, 7 and 10 °C min⁻¹. The Al₂O₃ standard was used to calibrate the dilatometer for each heating rate.

The XRD analysis was performed on the powder samples in the Bragg–Brentano geometry with CuK α radiation on the Seifert XRD7 diffractometer. The point detector was used to detect the diffracted beam, and the diffraction patterns were measured with a step of 0.05°.

Microstructure observations were performed using the FEI QuantaTM FX200 scanning electron microscope with an accelerating voltage of 10 kV in low vacuum mode (100 Pa). The micrographs were taken from fracture surfaces of samples.

Kinetic analysis

Calculation of kinetic parameters

The kinetic parameters were calculated using the Kissinger method, which is often used for crystallization kinetics [19, 20]. It is based on the following equation [21]:

$$\ln\left(\frac{\beta}{T_m^2}\right) = \text{const} - \frac{E_A}{RT_m}, \quad (1)$$

where β is the heating rate, T_m is the temperature at which the process has maximum rate, A is the pre-exponential factor, E_A is the apparent activation energy and R is the universal gas constant. The value of E_A can be determined from the slope of the plot of $\ln(\beta/T_m^2)$ versus T_m^{-1} .

Next, the crystallization mechanism can be determined using the Avrami peak factor n_A which is defined as [16, 22–24]:

$$n_A = \frac{2.5T_m^2 R}{w_{1/2} E_A}, \quad (2)$$

where $w_{1/2}$ is the half-width of a peak.

Peak separation

For the separation of overlapping peaks, the Fraser–Suzuki function [25] was applied to the expansion rate curves (dTDA). It can be written as:

$$y(x) = a_0 \exp \left[- \ln(2) \left[\frac{\ln \left(1 + 2a_1 \frac{x-T_m}{w_{1/2}} \right)}{a_1} \right]^2 \right], \quad (3)$$

where a_0 , a_1 , T_m and $w_{1/2}$ are the height, asymmetry, position and half-width of the peak, respectively. Values of these parameters are found by using numerical optimization.

Results

According to the XRD results (see Fig. 1), the dominant mineral phase in the studied green samples is illite (80 mass%) and the major impurities are quartz (12 mass%), orthoclase (4 mass%) and montmorillonite (4 mass%). The reflections corresponding to the illite vanished at the temperature of 1100 °C. On the other hand, the quartz reflections are still visible along with a newly formed mullite phase. At 1300 °C, the peaks belonging to the quartz and the newly formed mullite phase are more significant and remain visible even at 1500 °C. In addition, at this temperature, the formation of a new phase, cristobalite, is observed. The increasing content of the amorphous phase with increasing temperature (especially at 1500 °C) is also observed.

The fracture surface of the green sample consists of aggregates of small flat grains of illite (see Fig. 2a). After thermal treatment at the temperature of 1100 °C (see Fig. 2b), the illite grains are still flat but thicker and smoother. The formation of mullite needles occurred at a higher temperature (1300 °C); see Fig. 2c. The results show that the mullite needles are getting thinner with increasing temperature up to 1500 °C (Fig. 2d).

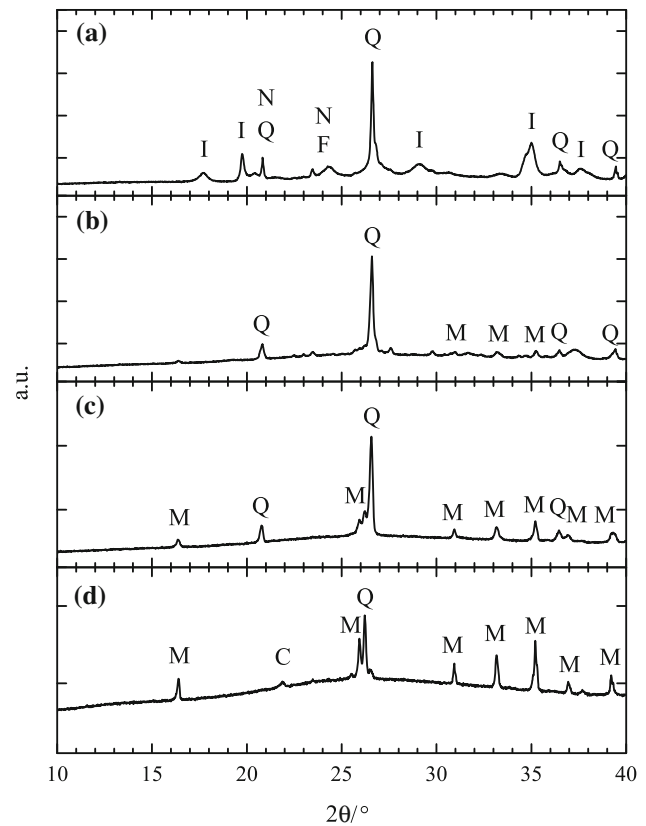


Fig. 1 XRD patterns of the green sample (a), sample fired at temperatures 1100 °C (b), 1300 °C (c), and 1500 °C (d) [I - illite, Q - quartz, F - K-feldspar (orthoclase), N - montmorillonite, M - mullite, C - cristobalite]

The results of the non-isothermal TDA up to 1300 °C with different heating rates are shown in Fig. 3. The first observed effect, in the temperature interval from 450 to 800 °C, corresponds to the dehydroxylation of illite, during which the structurally bound water leaves the crystal lattice [3]. After that, the crystal structure of illite remained almost unchanged up to ~ 950 °C where the shrinkage of the sample due to sintering is observed. According to the dTDA results (see Fig. 4), this process can be divided into two steps. The temperature region above ~ 1215 °C was not studied due to the effects of force (15 cN) which push on the sample in the dilatometer.

Peak separation

The peak separation procedure was applied to the dTDA curves after the baseline subtraction (see Fig. 5). This procedure allows determination of the values of T_m and $w_{1/2}$ for the reaction sintering of illite using numerical optimization. The values for the first and second steps of the illite sintering for different heating rates are shown in Table 1.

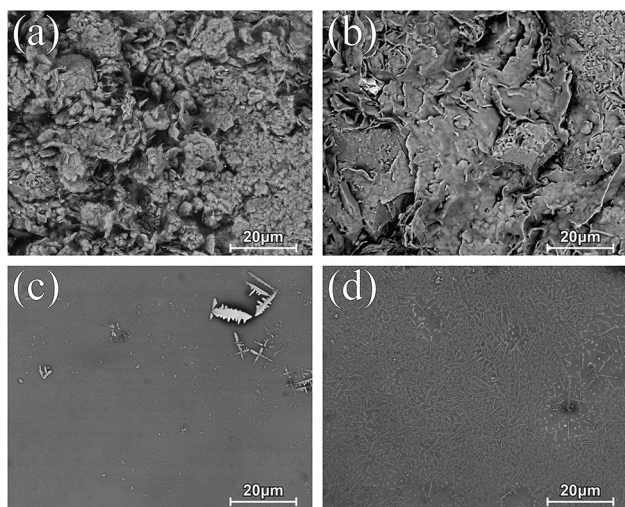


Fig. 2 SEM images of the fracture surface of the green illite sample (a), samples fired at temperature 1100 °C (b), 1300 °C (c) and 1500 °C (d)

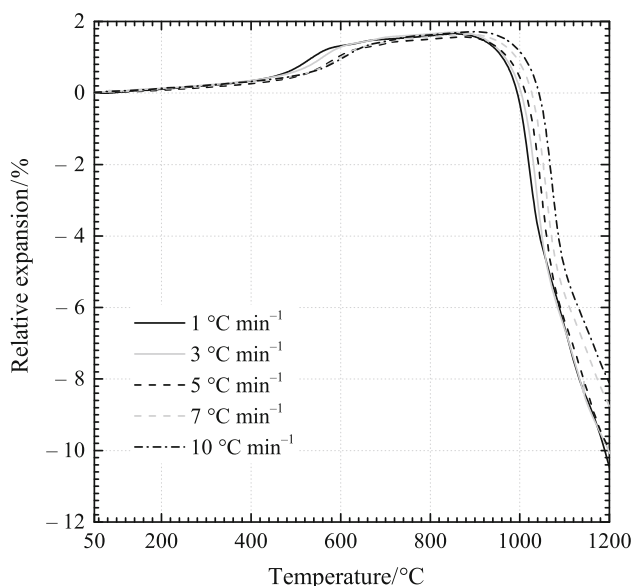


Fig. 3 Thermogravimetric curves of illite samples with various heating rates

Kinetic analysis

From the determined values of T_m of both processes (Table 1) with corresponding heating rates β , the Kissinger-type plot was made (see Fig. 6). As shown in Fig. 6, the Kissinger-type plots exhibit only one linear part, which indicates the independence of the values of apparent activation energy of both reactions on the heating rate. The determined value of the apparent activation energy for the first step of illite reaction sintering is $E_A = (625 \pm 18) \text{ kJ mol}^{-1}$ and for the second step is $E_A = (575 \pm 14) \text{ kJ mol}^{-1}$. On the other hand, the value of E_A

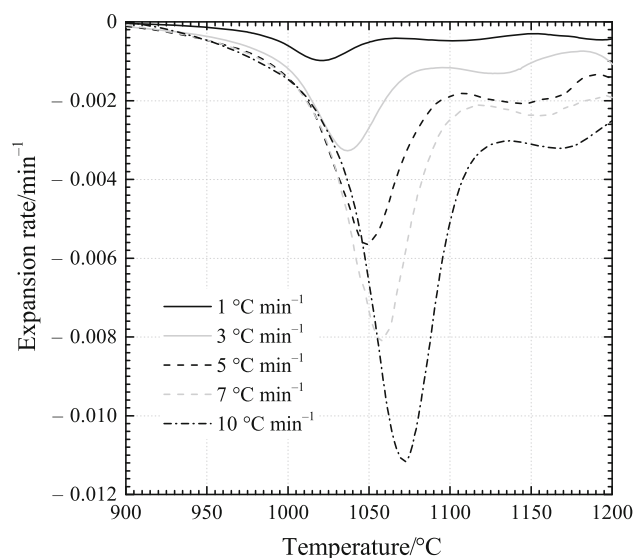


Fig. 4 Expansion rate curves (dTDA) of illite samples in the sintering region with various heating rates

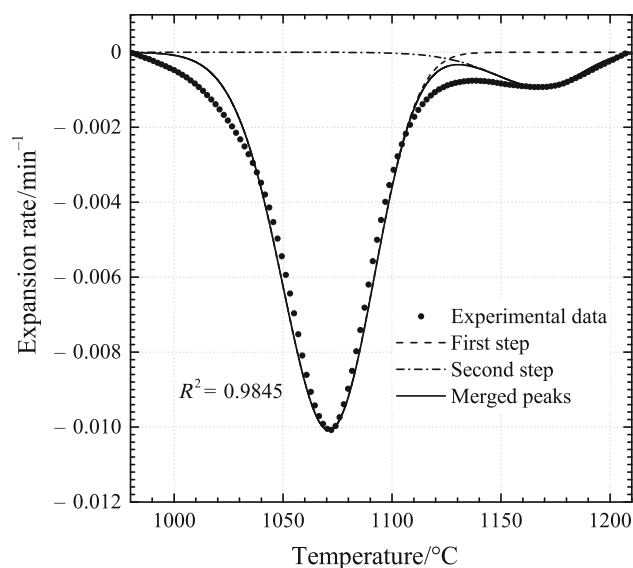


Fig. 5 An example of peak separation procedure for heating rate of 10 °C min^{-1}

for the first step is six times higher than the value reported in [6] (100 kJ mol^{-1}). However, the value of the apparent activation energy in the aforementioned study was calculated using the Arrhenius plot based on the measurements of the sample shrinkage after firing, which can cause large uncertainties. As the authors noted, due to the implication of different activated phenomena, the correlation factor is not close to one. The sintering mechanism was identified as viscous flow and the investigation was in the temperature interval from 850 to 1075 °C.

The average value of the Avrami peak factor ($n_A = 1.18 \pm 0.07$) for the first step (Table 2) suggested

Table 1 Values of T_m , and $w_{1/2}$ of the first and second steps of illite reaction sintering for different heating rates

$\beta/^\circ\text{C min}^{-1}$	First step		Second step	
	$T_m/^\circ\text{C}$	$w_{1/2}/^\circ\text{C}$	$T_m/^\circ\text{C}$	$w_{1/2}/^\circ\text{C}$
1	1018.82	51.64	1102.53	47.08
3	1035.39	49.60	1136.24	42.13
5	1047.74	50.83	1147.19	53.41
7	1056.66	45.58	1151.99	57.85
10	1070.04	49.31	1167.99	47.43

Table 2 Calculated values of n_A of the first and second steps of illite reaction sintering for different heating rates

$\beta/^\circ\text{C min}^{-1}$	First step	Second step
	n_A	n_A
1	1.08	1.34
3	1.15	1.57
5	1.14	1.26
7	1.29	1.17
10	1.22	1.46

long mullite needles [26]. This is in good agreement with the observation of illite by SEM (Fig. 2).

Conclusions

The sintering of illite was studied using non-isothermal therm dilatometric analysis under dynamic N_2 atmosphere. The kinetic analysis was carried out using the Kissinger method. The summary of the results is as follows:

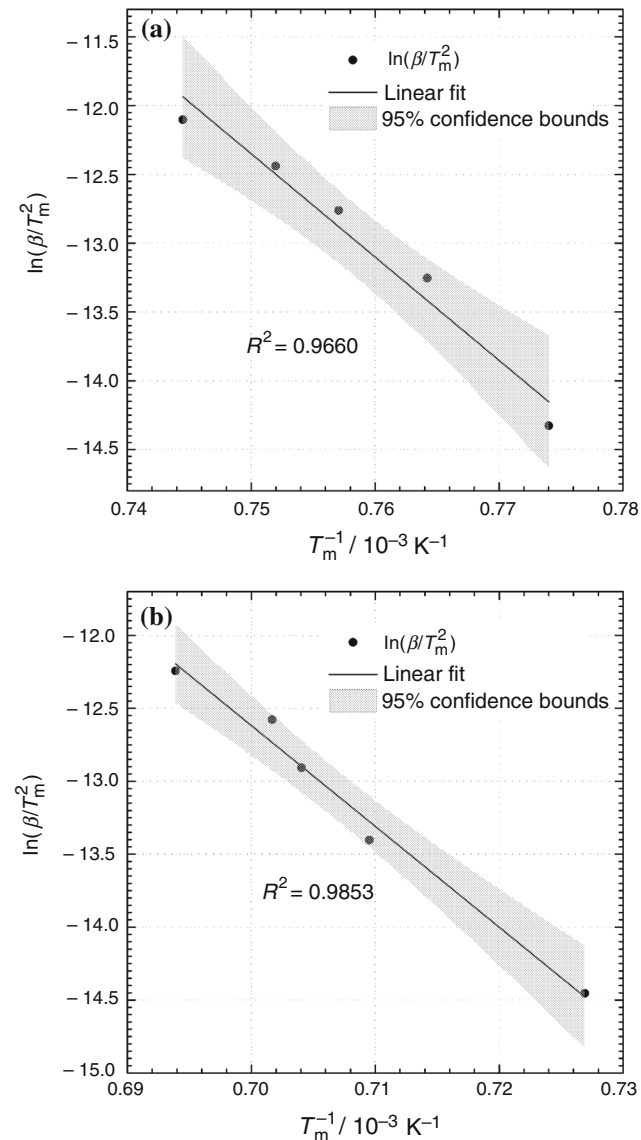
- The determined values of the apparent activation energy for the first and second steps are $E_A = (625 \pm 18)$ kJ mol^{-1} and $E_A = (575 \pm 14)$ kJ mol^{-1} , respectively.
- The values of Avrami peak factor for the first and second steps are $n_A = 1.18 \pm 0.07$ and $n_A = 1.36 \pm 0.14$, respectively.
- Based on these results, the first step can be characterized as the growth of plates of finite dimensions and the second step can be described as the thickening of long mullite needles.
- Results also show that the apparent activation energy of both steps is independent on the heating rate.

In this study, a kinetic analysis was employed to determine the mechanisms of illite reaction sintering for the first time. The results contribute to the basic knowledge about the sintering of wide-range ceramic products based on clay mineral illite. From a more practical perspective, the kinetic parameters can be used for the simulation and optimization of the sintering process. For this purpose, the pre-exponential factor must be determined in addition to the activation energy and Avrami peak factor. This is, however, relevant only for particular ceramic mixtures used for the production of ceramics.

Acknowledgements This research was supported by the Czech Science Foundation, Grant No. GA17-16772S.

References

1. Rice RW. Ceramic fabrication technology. Boca Raton: CRC Press; 2002.

**Fig. 6** Kissinger-type plots: **a** first step and **b** second step of illite reaction sintering

that this step can be characterized as the growth of plates of finite dimensions. The average value ($n_A = 1.36 \pm 0.14$) for the second step can be described as thickening of the

2. Kang S-JL. Sintering: densification, grain growth and microstructure. Oxford: Elsevier Butterworth-Heinemann; 2004.
3. Húlan T, Trník A, Medved' I. Kinetics of thermal expansion of illite-based ceramics in the dehydroxylation region during heating. *J Therm Anal Calorim.* 2017;127:1–8.
4. Bohor BF. High-temperature phase development in illitic clays. *Clays Clay Miner.* 1963;12:233–46.
5. Aras A. The change of phase composition in kaolinite- and illite-rich clay-based ceramic bodies. *Appl Clay Sci.* 2004;24:257–69.
6. Khalfaoui A, Kacim S, Hajjaji M. Sintering mechanism and ceramic phases of an illitic-chloritic raw clay. *J Eur Ceram Soc.* 2006;26:161–7.
7. Furlong RB. Electron diffraction and micrographic study of the high-temperature changes in illite and montmorillonite under continuous heating conditions. *Clays Clay Miner.* 1967;15:87–101.
8. Sedmale G, Sperberga I, Sedmalis U, Valancius Z. Formation of high-temperature crystalline phases in ceramic from illite clay and dolomite. *J Eur Ceram Soc.* 2006;26:3351–5.
9. Carroll DL, Kemp TF, Bastow TJ, Smith ME. Solid-state NMR characterisation of the thermal transformation of a Hungarian white illite. *Solid State Nucl Magn Reson.* 2005;28:31–43.
10. Wattanasiriwech D, Srijan K, Wattanasiriwech S. Vittrification of illitic clay from Malaysia. *Appl Clay Sci.* 2009;43:57–62.
11. Wang G, Wang H, Zhang N. In situ high temperature X-ray diffraction study of illite. *Appl Clay Sci.* 2017;146:254–63.
12. Ptáček P, Křečková M, Šoukal F, Opravil T, Havlica J, Brandštetr J. The kinetics and mechanism of kaolin powder sintering I. The dilatometric CRH study of sinter-crystallization of mullite and cristobalite. *Powder Technol.* 2012;232:24–30.
13. Emmerich W-D, Hayhurst J, Kaisersberger E. High temperature dilatometer study of special ceramics and their sintering kinetics. *Thermochim Acta.* 1986;106:71–8.
14. Knapek M, Húlan T, Minárik P, Dobroň P, Štubňa I, Stráská J, et al. Study of microcracking in illite-based ceramics during firing. *J Eur Ceram Soc.* 2016;36:221–6.
15. Húlan T, Trník A, Štubňa I, Bačík P, Kaljuvee T, Vozár L. Development of Young's modulus of illitic clay during heating up to 1100 °C. *Mater Sci Medzg.* 2015;21:429–34.
16. Ptáček P, Šoukal F, Opravil T, Nosková M, Havlica J, Brandštetr J. The kinetics of Al-Si spinel phase crystallization from calcined kaolin. *J Solid State Chem.* 2010;183:2565–9.
17. Liu YF, Liu XQ, Tao SW, Meng GY, Sorensen OT. Kinetics of the reactive sintering of kaolinite-aluminum hydroxide extrudate. *Ceram Int.* 2002;28:479–86.
18. Vyazovkin S, Burnham AK, Criado JM, Pérez-Maqueda LA, Popescu C, Sbirrazzuoli N. ICTAC Kinetics Committee recommendations for performing kinetic computations on thermal analysis data. *Thermochim Acta.* 2011;520:1–19.
19. Karamanov A, Pelino M. Sinter-crystallization in the diopside-albite system. Part II. Kinetics of crystallization and sintering. *J Eur Ceram Soc.* 2006;26:2519–26.
20. Lopes AAS, Monteiro RCC, Soares RS, Lima MMRA, Fernandes MHV. Crystallization kinetics of a barium-zinc borosilicate glass by a non-isothermal method. *J Alloys Compd.* 2014;591:268–74.
21. Kissinger HE. Reaction kinetics in differential thermal analysis. *Anal Chem.* 1957;29:1702–6.
22. Ondro T, Trník A. Kinetic behaviour of thermal transformations of kaolinite. In: AIP conference proceedings 2018;1988.
23. Ondro T, Trník A. Non-isothermal kinetic analysis of processes occurring during thermal treatment of kaolinite. In: AIP conference proceedings 2017;1866.
24. Augis JA, Bennett JE. Calculation of the Avrami parameters for heterogeneous solid state reactions using a modification of the Kissinger method. *J Therm Anal.* 1978;13:283–92.
25. Perejón A, Sánchez-Jiménez PE, Criado JM, Pérez-Maqueda LA. Kinetic analysis of complex solid-state reactions. A new deconvolution procedure. *J Phys Chem B.* 2011;115:1780–91.
26. Málek J. The applicability of Johnson-Mehl-Avrami model in the thermal analysis of the crystallization kinetics of glasses. *Thermochim Acta.* 1995;267:61–73.

Publisher's Note Springer Nature remains neutral with regard to jurisdictional claims in published maps and institutional affiliations.